Title

A Quantitative Spatiotemporal Atlas of Gene Expression in the Drosophila Blastoderm

Journal

Cell, 133(2)

ISSN

0092-8674

Authors

Fowlkes, Charless C

Hendriks, Cris L Luengo

Keränen, Soile VE

et al.

Publication Date

2008-04-01

DOI

10.1016/j.cell.2008.01.053

Peer reviewed

Cell

Resource

A Quantitative Spatiotemporal Atlas of Gene Expression in the *Drosophila* Blastoderm

Charless C. Fowlkes,[1,2] Cris L. Luengo Hendriks,[1,3] Soile V.E. Keränen,[1,4] Gunther H. Weber,[1,5] Oliver Rübel,[1,5] Min-Yu Huang,[1,5] Sohail Chatoor,[1,3] Angela H. DePace,[1,4] Lisa Simirenko,[1,4] Clara Henriquez,[1,4] Amy Beaton,[4] Richard Weiszmann,[4] Susan Celniker,[1,3] Bernd Hamann,[1,5] David W. Knowles,[1,3] Mark D. Biggin,[1,4] Michael B. Eisen,[1,4,*] and Jitendra Malik[1,6,*]

[1]Berkeley Drosophila Transcription Network Project
[2]Department of Computer Science, University of California, Irvine, CA 92697, USA
[3]Life Sciences Division
[4]Genomics Division
Lawrence Berkeley National Laboratory, One Cyclotron Road, Berkeley, CA 94720, USA
[5]Institute for Data Analysis and Visualization (IDAV) and Department of Computer Science, University of California, Davis, CA 95616, USA
[6]Department of Electrical Engineering and Computer Science, University of California, Berkeley, CA 94720, USA
*Correspondence: mbeisen@lbl.gov (M.B.E.), malik@cs.berkeley.edu (J.M.)
DOI 10.1016/j.cell.2008.01.053

SUMMARY

To fully understand animal transcription networks, it is essential to accurately measure the spatial and temporal expression patterns of transcription factors and their targets. We describe a registration technique that takes image-based data from hundreds of *Drosophila* blastoderm embryos, each costained for a reference gene and one of a set of genes of interest, and builds a model VirtualEmbryo. This model captures in a common framework the average expression patterns for many genes in spite of significant variation in morphology and expression between individual embryos. We establish the method's accuracy by showing that relationships between a pair of genes' expression inferred from the model are nearly identical to those measured in embryos costained for the pair. We present a VirtualEmbryo containing data for 95 genes at six time cohorts. We show that known gene-regulatory interactions can be automatically recovered from this data set and predict hundreds of new interactions.

INTRODUCTION

The output of animal transcription networks are dynamic, three-dimensional patterns of gene expression. It is a major challenge to decipher the transcriptional information encoded in animal genomes to the point where we can model and predict such patterns. Developing techniques that accurately characterize and analyze gene-expression patterns in the context of changing morphology is a critical step toward this goal.

Spatial patterns of protein and mRNA expression are being systematically recorded by various approaches over a range of spatial and temporal resolutions in several animal systems (e.g., Myasnikova et al., 2001; Tomancak et al., 2007; Kudoh et al., 2001; Tassy et al., 2006; Visel et al., 2004; Lein et al., 2007). These data sets, however, do not provide a comprehensive quantitative description of gene expression in a whole developing embryo at the spatiotemporal resolution needed for detailed computational modeling of animal-transcription networks in three dimensions. Perhaps the most comprehensive, automated expression atlas construction effort to date is of mouse brain imaged via serial sectioning and registered using anatomical features (Lein et al., 2007). This approach, however, currently yields relatively low temporal and spatial resolution (along the sectioning axis) and limited quantitation of gene expression.

To address the need for sufficiently high-resolution quantitative spatial expression data, we have previously developed methods, based on fluorescence microscopy, that measure relative concentrations of gene products in three dimensions over an entire *Drosophila* blastoderm embryo at the resolution of individual cells (Luengo Hendriks et al., 2006; Keränen et al., 2006) along with tools for interactively visualizing such data (Rübel et al., 2006; Weber et al., 2008).

A serious difficulty encountered in all current strategies for quantitating spatially resolved gene expression, including our own, is that it is not possible to label the expression of more than a few gene products in a given animal or tissue (e.g., Kosman et al., 2004). Yet, even simple portions of animal-transcription networks can comprise tens of regulators and hundreds of target genes (e.g., Oliveri and Davidson, 2004). A single *cis*-regulatory module (CRM) may often be bound by five, ten or even more colocalized regulators (e.g., Yuh et al., 2001). Therefore, to analyze how spatial and temporal changes in transcription factors correlate with changes in expression of their targets, it will be necessary to simultaneously compare the expression levels of many more gene products than is possible with conventional microscopy.

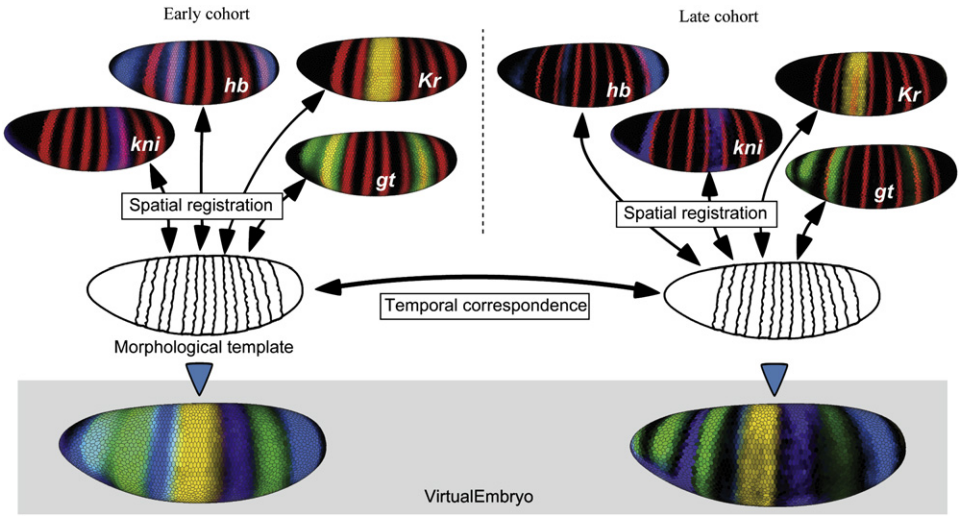

Figure 1. Data from Hundreds of Individually Imaged Embryos Is Averaged into a Composite VirtualEmbryo

On the top panel, each individual embryo is stained for nuclei, a common marker gene (red) and a gene of interest (second color). In the center panel, within each temporal cohort, the marker gene is used to guide *spatial registration* on to a *morphological template*; *temporal correspondences* between cohorts are provided by a model of typical nuclear movements. On the bottom panel, once correspondences across embryos have been established, expression measurements are averaged and *composited* to create a model *VirtualEmbryo* in which the expression of many genes can be analyzed.

In this paper, we present a computational technique that overcomes this limitation by compositing independent expression measurements made from images of hundreds of different embryos into a common spatiotemporal atlas in which the average expression patterns of many gene products can be studied simultaneously. Our technique involves two key components, outlined in Figure 1.The first is a spatial registration algorithm that uses a reference gene-expression pattern common to all labeled embryos to help identify equivalent corresponding cells or nuclei across images of multiple embryos at the same stage of development. The resulting correspondences are used to map expression measurements for other genes, whose expression was labeled in only a subset of embryos, onto a common model. The second component is a temporal registration method that uses a dynamical morphological template specifying the average positions and movements of cells or nuclei to provide correspondences between nuclei in embryos imaged at different developmental time points (Figure 1). Once correspondences have been established among embryos within and between cohorts, expression measurements are combined into a single composite model, termed a VirtualEmbryo, which describes the average patterns of expression for many genes at multiple time points (Figure 1).

In developing our method, we measured significant geometric variability between individual embryos at the same developmental stage both in their size, shape, number, and positions of nuclei and in the locations of gene-expression patterns. We show that our registration methods correctly take this geometric variation into account by demonstrating that the VirtualEmbryo accurately describes average patterns of gene expression present in individual embryos. Finally, to establish the utility of this comprehensive, quantitative, spatial expression data, we carry out a statistical analysis for a set of 17 regulatory factors and 95 target genes that recovers many known regulatory interactions from the literature and predicts many new ones.

RESULTS

Data-Acquisition Pipeline

Our previously established methods were used to obtain quantitative measurements of gene expression in individual embryos (Luengo Hendriks et al., 2006). Briefly, embryos were fixed and fluorescently stained to label the mRNA expression patterns of two genes and nuclear DNA. One of the genes labeled was either *eve* or *ftz*, which were used as fiduciary markers for subsequent spatial registration. Embryos were manually staged into one of six temporal cohorts and imaged by two-photon microscopy. Using the DNA marker, the location and extent of each blastoderm nucleus was automatically determined, and its 3D location was recorded along with the average fluorescence levels of the two genes in the nucleus and surrounding cytoplasm. The resulting data structure, which we call a PointCloud, was generated for 1822 embryos, including 95 genes and spanning the 50 min prior to the onset of gastrulation.

Spatial Registration of PointClouds

Analysis of the PointCloud data suggests that even embryos at approximately the same developmental stage vary quite significantly in their size, shape, number, and distribution of nuclei, and in the relative spatial locations of gene-expression patterns (e.g., Figure 2). This geometric variability in the data describing individuals must include true biological variations among embryos as well as measurement errors and physical deformations introduced by our methods.

For example, the PointCloud data showed that the embryos imaged ranged in overall egg Length from 301 μm to 502 μm

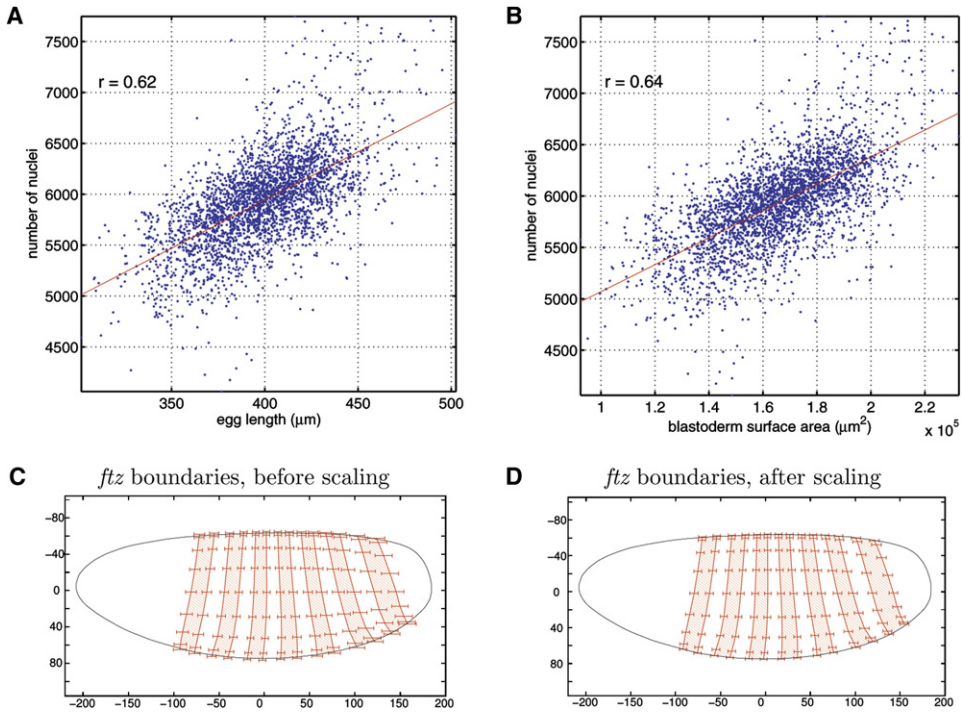

Figure 2. Variations in Blastoderm Size, Number of Nuclei, and Gene-Expression Stripe Locations between Embryos

(A and B) Scatter plots in which embryo length (A) and surface area (B) are both correlated with the number of nuclei (y axis), demonstrated here with a linear fit (red line). Because experimental errors in nuclear count should not correlate with errors in determining surface area or egg length, these correlations likely represent true biological variability among embryos.

(C and D) The variability in the location of *ftz* gene expression stripe locations before (C) and after (D) embryos are scaled to the average cohort egg length just prior to gastrulation (stage 5:75%–100% cell-membrane invagination). The plots are orthographic projections in which the anterior of the embryo is to the left, the dorsal midline to the top, and the center of mass of the embryo is at the origin. Each line specifies the average stripe boundary location with error bars showing one standard deviation in the A-P coordinate. Prior to scaling embryos to a common length, standard deviations for *ftz* stripe locations are as large as 11.1 μm, or 62% of the average *ftz* stripe width. After scaling by egg length the variation is reduced but is still significant (std dev up to 5.4 μm, or 30% of average stripe width).

(mean = 398 μm, standard deviation = 29.4 μm). Although some of this size variation certainly results from the fixation, staining, and mounting procedures the embryos were subjected to, much of it likely represents true biological variation since egg length and blastoderm surface area showed a marked correlation with the total number of peripheral nuclei (r = 0.62 and r = 0.64, Figures 2A and 2B). While our counts of nuclear number (which exclude yolk nuclei and pole cells) are also subject to some small error on the order of a few percent (Luengo Hendriks et al., 2006), these errors are too small to explain the measured variation and should not correlate with egg length or surface area. Thus, significant biological variation in the shapes of individual embryos must exist prior to any experimental manipulation. Indeed, the variation in embryo size we measured is comparable to reports for embryos that have not been fixed and stained (Warren, 1924; Azevedo et al., 1996), and our automated counts of nuclei number are comparable to those derived from manual counting of nuclei in a few embryos (Zalokar and Erk, 1976; Turner and Mahowald, 1976).

Such large geometric variation makes comparing gene expression among individuals nontrivial, as some technique more sophisticated than simply overlaying embryos is required to identify equivalent corresponding cells in different embryos. Unlike the adult animal, the blastoderm lacks distinctive morphological features that identify particular cells or tissues. Instead, nuclei are primarily distinguished by the expression levels of transcription factors and other regulators that control development, including the genes whose expression we measured. Therefore, our spatial registration method seeks to identify corresponding nuclei in different embryos, which have similar gene-expression profiles.

To perform spatial registration, we first use data from all PointClouds in each temporal cohort to build a morphological template with a fixed number of nuclei arranged to match the average measured nuclear distribution and mean embryo shape. The template also specifies the mean locations of the *ftz* and *eve* marker gene-expression boundaries (Figure 1). We compute a smooth deformation of each individual PointCloud to warp both the extracted marker gene boundaries and the overall PointCloud shape into alignment with the template (see Figure 3). For each nucleus, a best match in the template is identified, establishing correspondences for all cells across all embryos in the cohort. Once detailed correspondences among embryos have been found, estimates of the average locations of marker genes specified in the template are refined and the spatial registration process repeated until further iterations provide no significant changes in the correspondence.

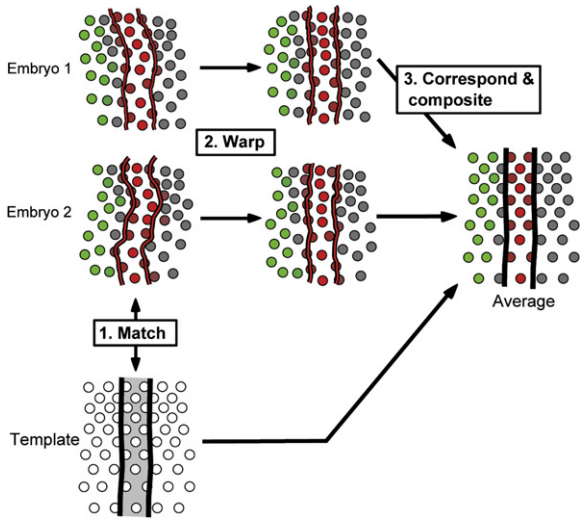

Figure 3. Fine Registration and Compositing Expression Values

A marker gene-expression pattern (red) is used to identify corresponding nuclei in different embryos and perform fine spatial registration. Each individual PointCloud is warped to bring extracted marker gene boundaries (red lines) into alignment with a standard morphological template (black lines). Individual per-nucleus measurements (here both red and green) are then composited onto the template to produce an estimate of average expression.

An initial estimate of the deformation required to bring PointClouds of a given cohort into register with the template was computed by automatically identifying the anterior-posterior (A-P) axis and scaling the PointClouds to the average egg length for that cohort. To establish the dorsal-ventral (D-V) orientation, the location of the ventral midline was judged by eye using gene expression and morphological markers. While this coarse alignment step did bring the embryos into closer alignment, factoring out gross variations in overall size, significant differences remained in the locations of expression patterns, as well as residual differences in PointCloud shape and the distribution of nuclei. For example, Figures 2C and 2D shows the standard deviation in the A-P locations of *ftz* expression boundaries before and after scaling embryos to the average egg length. Measuring expression boundaries with respect to egg length removes up to half the apparent variability in some stripe boundary locations, but standard deviations after scaling are still near 30% the average stripe width.

To factor out this remaining nonrigid geometric variation, we next carried out a fine registration step in which the embryos in each temporal cohort were warped onto the morphological template using automatically detected boundaries of either *ftz* or *eve* expression domains as markers (Figure 3; see Experimental Procedures). Once all PointClouds had been warped into alignment, each nucleus in the morphological template was matched to the nearest PointCloud nucleus. This many-to-one matching, which allowed multiple nuclei in the template to correspond to the same detected nucleus, is appropriate since the total number of nuclei varies across embryos.

The warping of individual PointClouds during fine registration not only establishes more accurate correspondences between cells, but also provides an estimate of the geometric variation among PointClouds, excluding that component due to isotropic variation in size which was removed by coarse alignment (see Figures S1 and S2).

Registration between Temporal Cohorts

To track the temporal dynamics of gene expression, it is necessary to estimate correspondences between the nuclei in successive temporal cohorts. While there are no nuclear divisions during the 50 min period spanned by our cohorts, expression patterns of *eve*, *ftz*, and many other genes move relative to the lattice of nuclei, and thus marker gene boundaries cannot be used to identify corresponding nuclei over time (Keränen et al., 2006). Furthermore, based on nuclear tracking in live imaging and nuclear density measurements from fixed material, we found that nuclei flow from the anterior and posterior poles toward the dorsal surface while elongating basally (Keränen et al., 2006). Previous models of the *Drosophila* blastoderm have tacitly assumed that a unique spatial coordinate identifies the same cellular/nuclear location at different times (e.g., Jaeger et al., 2004). Our results clearly indicated this assumption is not valid as localized contractions or expansions of the blastoderm surface mean some nuclei consistently travel as far as three cell diameters during stage 5 (Keränen et al., 2006).

To take these nuclear movements into account in establishing correspondences across cohort templates, we developed a method to infer nuclear movements from fixed material (Fowlkes and Malik, 2006). The average embryo shape and nuclear density pattern from each cohort was used to constrain a numerical model that predicted the direction and distance each nucleus needed to move through space to account for the measured changes in density and shape between cohorts. The resulting morphological template time series, which specified the locations of 6078 nuclei for each of the six temporal cohorts, was used for spatially registering and compositing expression data as described above. This provided the needed correspondences between nuclei at different time points.

Compositing Expression Levels onto the VirtualEmbryo

Before averaging expression levels for each gene onto the morphological template, it was necessary to put fluorescence measurements from different embryos onto a common scale. While our data provide an accurate measure of relative mRNA expression levels of a gene within an individual embryo (Luengo Hendriks et al., 2006), our methods result in variation in the absolute fluorescence between different embryos. In particular, the absolute degree of fluorescence varied significantly across embryos stained in different batches, presumably due to variable reaction time, efficiency, and other experimental artifacts.

To mitigate this error, we normalized mRNA expression levels for each gene across multiple batches and then averaged peak expression levels for each gene across all embryos within each temporal cohort to estimate the degree of total up- or downregulation between cohorts (see Experimental Procedures). As Figure S3 shows, the relative temporal changes in averaged fluorescence levels measured for each gene were reasonably consistent across staining batches. These expression time courses matched general expectations based on other data, suggesting that absolute differences in fluorescence provide a useful estimate of relative changes in expression levels between cohorts.

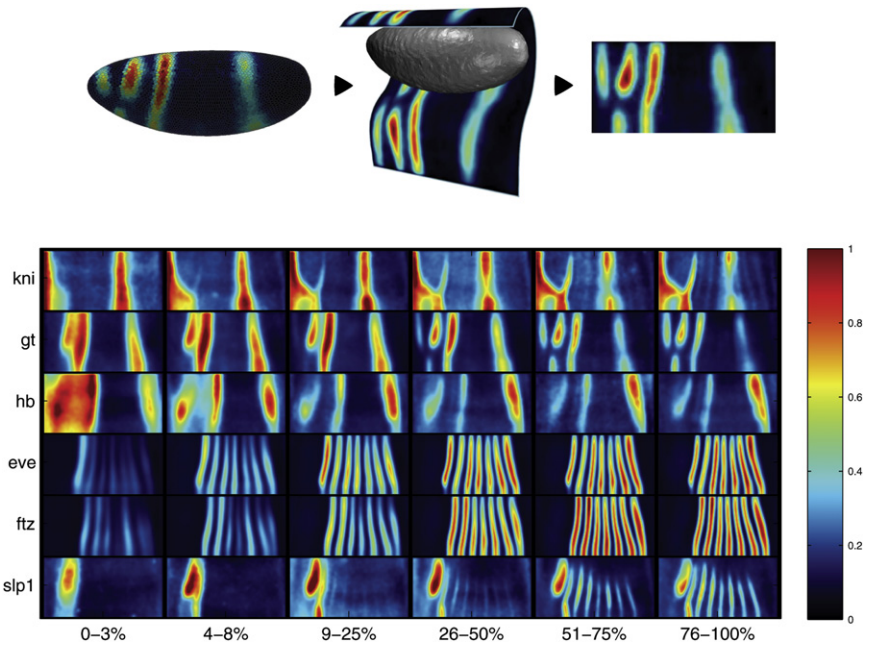

Figure 4. Examples of Average Temporal Patterns of mRNA Expression Recorded in the VirtualEmbryo for Several Gap (*kni,gt,hb*) and Pair-Rule (*eve,ftz,slp1*) Genes

Temporal cohorts, staged by percent membrane invagination, are arranged from left to right with each row corresponding to a different gene. Each rectangle shows a lateral view of the blastoderm in a half-cylindrical projection with the dorsal midline at top, the ventral midline at the bottom, and anterior to the left (see also Figures S4, S5, and S6).

To remove any remaining differences in the quantitation of each gene between embryos within a cohort, we chose a scale and offset for each embryo that minimized the average standard deviation in expression between embryos, subject to the constraint that the maximum average expression level matched the estimated time course. The scaled expression data for each gene from each PointCloud was then transferred to the corresponding nuclei in the appropriate cohort template and averaged together.

A Spatiotemporal Atlas of Gene Expression

The result of registration and compositing is a VirtualEmbryo that describes the average dynamics of gene expression and morphology in the blastoderm. Figure 4 shows example lateral views of the final average expression patterns recorded in the VirtualEmbryo for several genes displayed in cylindrical projection. Figure S4 shows the complete set of mRNA patterns for 95 different genes estimated from 1822 embryos and over 11 million cells. The genes analyzed include many known early acting transcription factors that specify patterning prior to gastrulation in *Drosophila*. For 23 of these factors, we have combined mRNA data from 25 or more embryos spanning the entire 50 min leading up to gastrulation. For the remaining 72 genes, which are known or putative targets of these early transcription factors, we have collected mRNA data from a smaller number of embryos, primarily in the three temporal cohorts just prior to gastrulation.

In addition to the average description present in the VirtualEmbryo, we also provide the individual raw PointClouds, files recording the nuclear correspondences identified between each individual PointCloud and the VirtualEmbryo, and associated metadata. We refer to this comprehensive data set as a "gene-expression atlas." Our VirtualEmbryo and the initial atlas release are publicly available through a web-based interface hosted at http://bdtnp.lbl.gov. We also provide a comprehensive visualization tool for examining relationships between different gene-expression patterns (Figures S6 and S7) (Rübel et al., 2006; Weber et al., 2008).

Evaluating Registration Accuracy

It is nearly impossible to judge by eye if the correspondence we have determined between nuclei in two different embryos is "correct," as most blastoderm nuclei lack any identifying morphological features. Since our method for determining correspondences is based on finding equivalent nuclei using gene-expression data, one objective criterion we have used to evaluate registration accuracy is to measure the extent to which nuclei from different individuals identified as corresponding have similar expression profiles. A second evaluation criterion we have used is to measure how accurately the mean expression data in the VirtualEmbryo captures the relationships between transcriptional regulator and target gene-expression patterns, as compared to individual embryos directly costained for the target and the regulator. We describe both approaches below.

Registration Decreases the Apparent Variation in Expression between PointClouds

First, we examined the effect of registration on the apparent variation in expression levels for reference and nonreference genes. Figures 5A and 5B shows the mean and standard deviation in expression levels at a given time point (stage 5: 50%–75%) for three different genes along a lateral A-P strip (n = 100, 25, and 8 embryos for *ftz*, *slp1*, and *gt*, respectively). For comparison, the variation in expression is plotted when nuclear correspondences have been determined by coarse alignment alone, i.e., assuming nuclei at the same relative spatial location along the A-P axis correspond (Figure 5A). We quantified the apparent interembryo variation in expression for each gene in a cohort by averaging the standard deviation across all corresponding nuclei in each PointCloud containing data for the gene (Figures 5A and 5B, top right of each panel; Table S1). The apparent interembryo variation is lower when correspondences are derived from fine registration rather than coarse alignment alone. Furthermore, after fine registration, our estimates of the average patterns become less "blurry" and more like those observed in individual embryos, particularly for highly modulated pair-rule patterns (e.g., *ftz* and *slp1*).

The decrease in apparent variability of our registration marker (here, *ftz*) suggests that our fine registration accurately identified corresponding *ftz* boundaries and warped them into alignment.

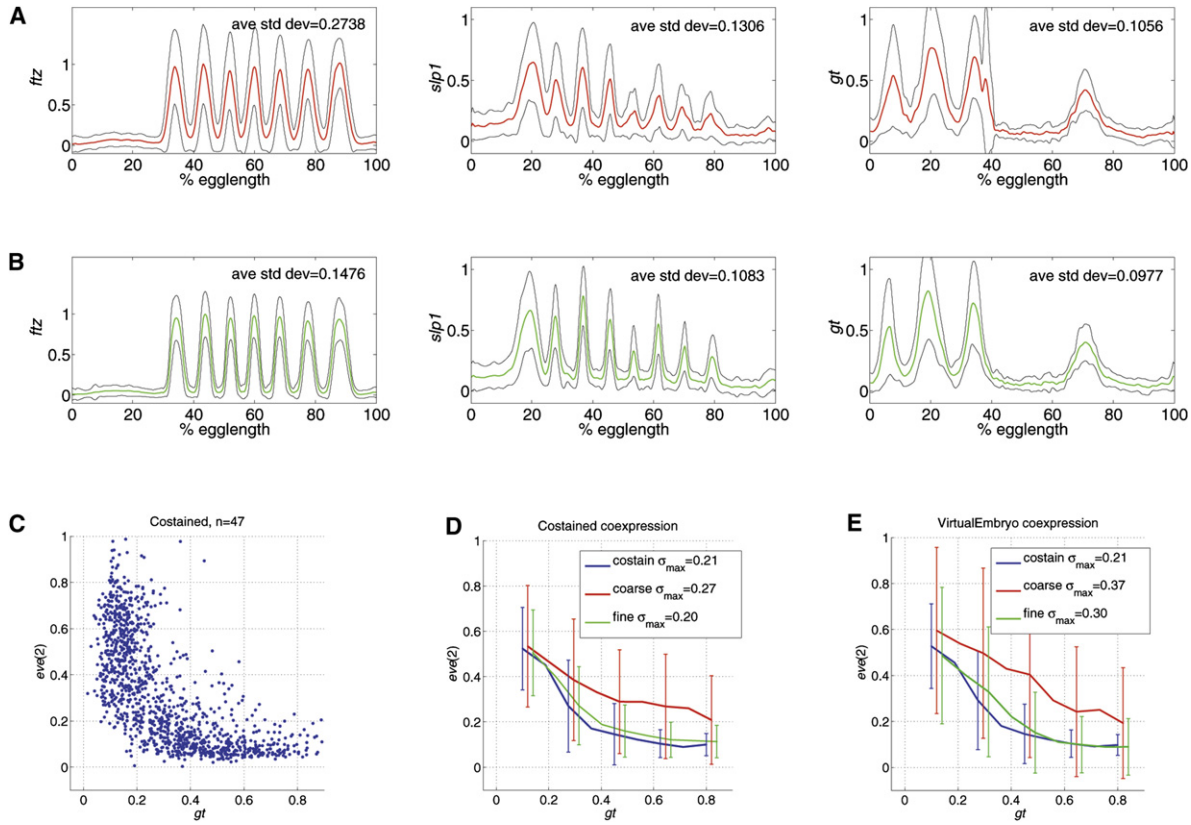

Figure 5. Fine Registration Removes Measured Interembryo Geometric Variability and Produces Average Regulatory Relationships Comparable to Those Measured in Individual Costained Embryos

(A and B) The mean and standard deviations for anterior-posterior expression profiles taken from a lateral strip before (A) and after (B) fine registration for three genes: *ftz* (n = 100), *slp1* (n = 25) and *gt* (n = 8). The interembryo variability decreases significantly with fine registration, both for the marker gene (*ftz*) but also for "held out" expression patterns (*slp, gt*). Inset numbers for each gene give the standard deviation averaged over the entire embryo.

(C) The coexpression of *gt* and *eve* near the dorsal surface along the anterior edge of *eve* stripe 2 in embryos costained for *eve* and *gt* (n = 47).

(D) The regulatory effect of *gt* on *eve* (2) inferred from costained (blue curve) embryos by binning nuclei based on the expression level of *gt* and computing the mean and standard deviation of *eve* expression for each bin. The red and green curves show the regulatory relation estimated by sampling pairs of nuclei in similar spatial locations after coarse alignment (red) and fine registration based on *eve* (green).

(E) The regulatory effect inferred from nuclei in different batches of embryos stained for either *eve* (n = 35) or *gt* (n = 28), which were identified as corresponding based on coarse alignment (red) or fine registration (green) using *ftz.* The costain estimate (blue curve) is repeated for comparison. The inferred relation based on registered embryos is quite close to the true coexpression measured in costained embryos. The variation in the regulatory relation across embryos in the virtual coexpression estimate is significantly smaller than the coarse registration and is nearly as small as the lower bound set by the level of variability quantified in individuals.

More importantly, the apparent interembryo variation also decreased for "held out" expression patterns (e.g., *slp1* and *gt*), which were not used during the fine registration process, indicating that registration makes good predictions about how all nuclei should be shifted based only on how the nuclei near *ftz* or *eve* boundaries are shifted. Table S1 shows the change in apparent variability between coarse alignment and fine registration for 23 early factors. The decrease in variation holds true for most of these genes and time points. One general exception is D-V patterning genes, suggesting that the precise locations of D-V expression boundaries are fairly uncorrelated with our A-P registration markers.

While this analysis shows that fine registration yields better correspondences than coarse alignment alone, it does not address what fraction of the remaining variation in expression between individuals after fine registration is due to remaining geometric variability and what fraction is attributable to nongeometric causes. Even a perfect registration algorithm would necessarily leave behind some variability due to measurement error in expression levels or genuine variability in the response of targets to their regulators (Gregor et al., 2007). If we could determine the amount of such nongeometric variability, this would provide a bound on how much, if at all, our registration algorithm could be further improved.

To experimentally establish a baseline on the nongeometric variability measured among embryos, we directly estimated the relation in expression levels between pairs of genes in individual embryos costained for both genes. This measurement is invariant to spatial deformations of the individual embryos, so any variability measured in the coexpression across costained

embryos must arise from nongeometric sources. We can directly compare the variability in this relation to that inferred by registering data from pairs of embryos in order to judge how much geometric variability remains after registration.

Figure 5C shows the relation in expression levels of *eve* and *gt* within a three-cell-wide lateral strip at the anterior boundary of *eve* stripe 2 in embryos costained for both *eve* and *gt.* Each point in the plot gives the joint expression level measured in a single nucleus from 1 of 44 embryos at stage 5:9%–75%. It is known that *gt* plays a key role in determining the anterior boundary of *eve* stripe 2. This regulatory relationship is revealed in the tight anticorrelation between the two genes' expression in this part of the embryo (Figure 5C). The blue curve in Figure 5D shows the average relation between the two factors estimated by binning nuclei based on the level of *gt* expression and then computing the average level of *eve* for each bin. The variability in the relation between the two genes was quantified by computing the standard deviation for *eve* expression in each bin. We measured a maximum standard deviation of 0.21 (relative to a maximal *eve* expression of 1). This measure of local variability is comparable in magnitude to similar measurements made on the relation of *bcd* and *hb* (Gregor et al., 2007). Because this variation is measured within individual embryos, it cannot be due to geometric variation and thus is not removable by our registration method. Instead, this variation is likely due to some combination of variability in the regulation of *eve* by *gt*, spatial variations in other unmeasured regulatory factors that also influence *eve* expression, and error in our measurements of mRNA concentrations.

Having set an upper bound for nongeometric variation, we then used the costained embryo data to quantify the effect of geometric variation between embryos on the apparent relationships between regulator and target expression in coarsely registered embryos. Pairs of costained embryos were selected at random, and the level of *eve* in one nucleus was compared to the level of *gt* in a nucleus at a corresponding spatial location in the other embryo. The red curve in Figure 5D shows that the resulting estimate of coexpression in coarsely aligned embryos is significantly different from that derived from individual costained nuclei with much greater apparent variability. In contrast, for pairs of nuclei from different embryos identified as corresponding by the fine registration process (using *eve* as the reference), the resulting curve (green in Figure 5D) is very similar to the direct costain curve and has small apparent variability. This implies that while the exact location of *eve* stripe two varies significantly from one embryo to the next (similar to *ftz* in Figure 2), the pattern of *gt* is shifted in a correlated manner. Table S1, which specifies the change in the apparent variability of individual genes before and after fine registration thus characterizes the extent to which expression patterns of individual genes are correlated with those of our registration markers.

Expression Relationships Are Similar in Costained Embryos and Registered PointClouds

Since most genes are spatially correlated with our registration marker in individuals, this suggests that the composite VirtualEmbryo data should accurately capture average regulatory relationships between individual genes. We verified this experimentally as displayed in Figure 5E, which shows the coexpression levels for *eve* and *gt* estimated from a VirtualEmbryo constructed using embryos stained for either *eve* and *ftz* or *gt* and *ftz* and registered on *ftz*. As the green curve in Figure 5E shows, even though *gt* and *eve* are never observed in the same embryo, the mean functional relationship inferred from the virtual coexpression measurements is quite close to that inferred from costained embryos. The resulting average estimate deviates from the costain estimate by less than 7% of the maximum expression level and has a maximum standard deviation of 0.30. In contrast, coarse alignment alone yields an average relation with a different shape (red curve, Figure 5D) and larger variability (max standard deviation = 0.36). Further analysis suggests our estimates of the variability remaining after registration may be quite conservative (see Supplemental Data).

In summary, the results of testing our two evaluation criteria suggest that the registration process successfully factors out a large fraction of the geometric sources of variability, leaving an average estimate of expression which is quite close to that measured in individual embryos.

Inferring Regulatory Interactions from Spatiotemporal Expression Data

One of our chief motivations for developing the blastoderm expression atlas is to help determine which transcription factors regulate which target genes. Expression patterns of regulators frequently correlate, at least in some portion of an animal, with those of their target genes. For example, the anticorrelation of *gt* expression with the anterior border of *eve* stripe 2 described previously (Figure 5). In principle, it ought to be possible to infer regulatory relationships by searching for such correlations. While such inferences cannot be taken on their own to indicate that a transcription factor directly binds and regulates a target gene, when combined with other classes of data such as genome-wide in vivo binding data and in vitro DNA specificity data, they should provide a significant constraint on possible models for the regulatory network.

To demonstrate the utility of the composite expression atlas for inferring regulatory interactions, we performed a regression analysis to predict regulatory interactions based solely on the spatial expression data. For each of the 95 genes contained in the atlas, we searched for a small set of regulators that best predicted that target gene's spatiotemporal dynamics. Because the individual components of blastoderm expression patterns (e.g., each stripe) are often controlled by distinct *cis*-regulatory modules (CRMs) (e.g., Clyde et al., 2003), we automatically segmented each target output pattern into individual expression domains and fit each such "module" independently, assuming that expression elsewhere was zero. This let us use a simple form for the regulatory function (see Experimental Procedures), while still allowing, for example, KR to repress *eve* stripe 5 but activate *eve* stripe 3. To limit the effects of overfitting, we selected the best 6 regulators from a pool of 17 known early-acting transcription factors by exhaustive feature selection, choosing that set of 6 regulators that best predicted the each target module pattern (largest R^2). Because protein expression patterns differ both spatially and temporally from mRNA expression patterns, we either used measured protein expression data (for BCD, HB, GT, or KR, see Figure S5) or inferred the protein patterns from their

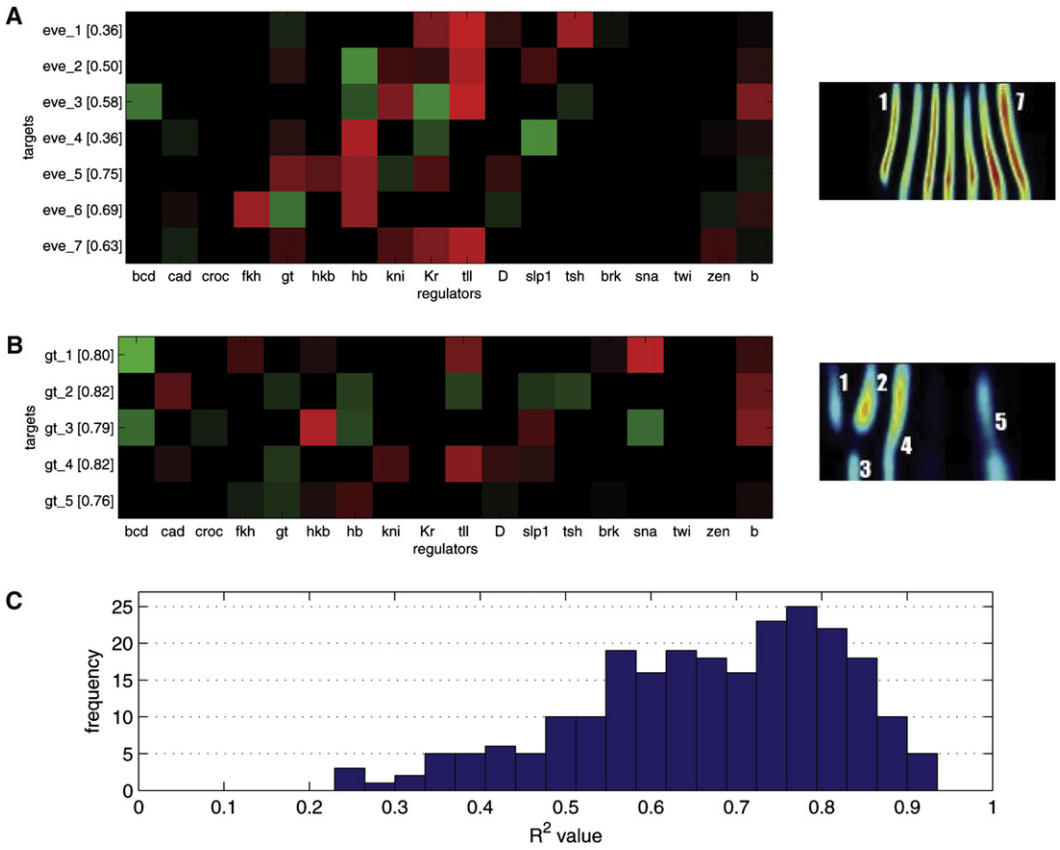

Figure 6. Regulatory Relationships Inferred from Composite Spatiotemporal Expression Data

(A) The coefficients for each of 17 regulators (columns) determined by fitting each target *eve* stripe (rows). Each row contains six nonzero entries corresponding to the selected regulators, which best predict the spatiotemporal expression of that target. Green indicates activation, red indicates repression, black indicates no interaction. The right-most column indicates the constant offset *b*. Quality of fit (R^2) values are specified in brackets.

(B) The coefficients for the individual components of the gap gene *gt*, ordered by A-P location.

(C) The distribution of R^2 fit values for all "modules" in the atlas (see Figure S6).

mRNA expression based on a fixed temporal delay of two cohorts (roughly 16 min).

Figures 6A and 6B shows the regression coefficients of each of 17 regulators (columns) determined by the fitting process for each target *eve* and gt stripe (rows). Green indicates predicted activators, red indicates repressors, and black indicates unused regulators (zero entries). Figure S8 shows similar fits for all 238 modules of the 95 genes in the atlas, and Figure 6C summarizes the distribution of R^2 values for all modules.

Broadly speaking, the R^2 goodness-of-fit values demonstrate that we can fit much of the expression data quite well with our relatively simple linear model. Of the 238 modules, 202 (85%) were fit with an R^2 value of 0.5 or greater. This suggests that this small set of 17 regulators contain enough spatial information to generate the wide variety of cell-expression profiles that are apparent by the end of stage 5.

In addition, the regression analysis contains many correct predictions. For example, the analysis correctly predicts HB as an activator of *eve* stripe 2 and KR, KNI, and GT as repressors (Small et al., 1992; Arnosti et al., 1996). Similarly, for *gt* stripe 5, the analysis correctly predicts repression by HB and Huckebein (Eldon and Pirrotta, 1991). Interestingly, the analysis also predicts regulation of A-P target genes by D-V regulators. For example the *gt* stripes clearly have a D-V pattern, which is picked out by the regression (regulation by SNA and BRK).

Not surprisingly, this model also has some clear failures. For example, BCD does not appear as an activator in many cases, including for one of its best-characterized targets, *eve* stripe 2. This is not surprising, since the analysis favors regulators whose protein expression changes sharply near boundaries of the target pattern, while BCD has a graded expression pattern. Another limitation is that the expression modules that we automatically identified may not correspond to the output of distinct CRMs. For example, in *eve*, stripes 4 and 6 are both controlled by the same regulators acting via a single CRM and stripes 3 and 7 both by another CRM (Clyde et al., 2003). This may in part explain the relatively poor quality of fits in Figure 6A to these stripes.

Finally, the comparison of the regression-analysis predictions to results in the literature underlines the well-known difficulty in correctly divining regulatory interactions within this complex network. For example, our analysis predicts SLP as a regulator of several *gt* stripes, and yet in *slp* loss-of-function mutant embryos, *gt* expression is not affected (Eldon and Pirrotta, 1991). Such loss-of-function genetic experiments, however, cannot

rule out the possibility of functionally redundant regulatory interactions, as revealed in other cases by more detailed experiments (e.g., Laney and Biggin, 1996), and thus cannot disprove predictions of our regression analysis. This and other complexities of the system suggest that picking apart network interactions will ultimately require careful consideration of multiple data sets.

DISCUSSION

Our work establishes a spatiotemporal quantitative atlas of gene expression and morphology for a whole embryo at cellular resolution. By using registration to bring quantitative gene-expression data for many genes into a common spatiotemporal frame, our methods open the way for quantitative analyses of the large networks of interactions between developmental regulators and their targets.

Accuracy of Registration

In general, registration techniques are designed to establish correspondences by factoring out a certain class of variations between individuals (typically geometric variation in, for instance, size and shape) while maintaining other variations of interest. Characterizing the performance of a particular algorithm, however, is conceptually difficult since the actual nature of the variations under study is seldom known in advance. Our analysis suggests that the registration method presented here comes close to separating geometric variability from the regulatory variability with which promoters in different cells respond to similar concentrations of transcription factors, at least to within the accuracy afforded by our measurement techniques. Factoring out geometric variability will be important in isolating and characterizing differences in regulatory mechanisms, both within and between closely related species.

Our results suggest that the registration procedure yields a VirtualEmbryo containing average expression data that are nearly as accurate as could be obtained from averaging directly costained embryos and is thus sufficient for many types of analyses of regulatory interactions. Such "virtual multiplexing" makes it practical to examine the relations in expression between any subset of genes without directly costaining embryos for all possible pairs.

Variation between Individuals

By identifying corresponding cells, our method allows the direct comparison of the locations and expression profiles of homologous cells in different individuals. This provides a computational tool for understanding biological variability arising from genetic, environmental, and stochastic sources within a population. Indeed, as a natural outcome of the development of our registration method, we have already measured several important aspects of variation between individual blastoderm embryos. Although some of the variation measured must represent experimental error, as discussed earlier, a significant percent of the measured differences clearly reflect real biological differences between embryos.

For example, we have estimated a quantitative upper bound on the degree of regulatory variability in the relationship between *gt* and its repression of the target CRM *eve* stripe 2. The values we measure are largely consistent with the earlier work of Gregor et al., who made a similar estimate for the variability in HB protein concentration as a function of BCD (Gregor et al., 2007).

We have also provided analogous upper bounds on the degree of geometric variability. In particular, we discovered there is a significant correlation between the number of nuclei and size of the embryo. Although this has not previously been reported, it is consistent with earlier results from embryo ligation experiments, suggesting that the number of nuclei and nuclear divisions are determined by some mechanism that senses local nuclear densities (Edgar et al., 1986). It is also consistent with the result of manipulation experiments in echinoderm and vertebrate embryos that suggest the ratio of cytoplasm to nuclear material regulates the number of cells at the midblastula transition (reviewed by Edgar et al., 1986). Our extensive measurements imply that among wild-type embryos that have not been experimentally manipulated, even modest changes in egg size likely influence the number of nuclear divisions/nuclear loss events.

Predicting Regulatory Interactions from Comprehensive Spatiotemporal Expression Data

The closest work to ours is that of Myasnikova et al. (2001) and Spirov et al. (2002), who registered spatial profiles of protein concentrations along the A-P axis of the *Drosophila* blastoderm using images of the lateral surface of embryos, which had been flattened before imaging. While their data only provides a 1D picture that largely disregards the blastoderm morphology, it has been widely adopted for use in modeling pattern formation due to its quantitative nature (e.g., Janssens et al., 2006; Ludwig et al., 2005). Our approach expands this quantitative picture of pattern formation with an explicit description of changing morphology and comprehensive coverage of many more spatially patterned genes, in full 3D.

We have demonstrated a technique for analyzing such 3D spatiotemporal expression data in order to uncover regulatory relationships between transcription factors and their targets. While our model of regulation is intentionally quite simple, it is capable of explaining many target patterns quite well with only a few regulators (as witnessed by high R^2 values for most of the targets). We are also able to recover many interactions proposed in the literature. While our model does not capture many potential subtleties of regulation such as cooperative or competitive interactions between multiple bound factors, posttranscriptional and translational control mechanisms, phosphorylation, etc., clearly it could be extended and made more accurate by including these processes (e.g., Clyde et. al., 2003; Struffi et. al., 2004).

Our long-term goal is to construct high-fidelity VirtualEmbryos containing protein and mRNA expression data for thousands of genes with the quantitative accuracy necessary to provide firm grounding for a new generation of developmental models that take into account features such as 3D diffusion and transport, nuclear movement, and interaction between A-P and D-V patterning systems. The availability of accurate 3D quantitative data at cellular resolution should provide far more constraints on potential models of the regulatory structures underlying animal development.

EXPERIMENTAL PROCEDURES

Imaging Individual Embryos

Individual embryos were fixed and fluorescently stained to label the mRNA and/or protein expression patterns of two genes and nuclear DNA, mounted on microscope slides and imaged using protocols in Luengo Hendriks et al. (2006). Additional antisense RNA probes were generated from PCR products of cDNAs in *Drosophila* Gene Collection I and *Drosophila* Gold Collection (for the list of used probes, see the online database at http://bdtnp.lbl.gov). For protein stains, the primary rabbit antibodies against BCD, KR, and GT were generated by BDTNP; the guinea pig antibodies against HB and KR were gift from J. Reinitz. The primary antibodies were detected using Alexa546-, Alexa555-, or Alexa610-conjugated secondary antibodies (Molecular Probes, 1:500).

Spatial Registration

For each temporal cohort, we used the template consisting of *eve* or *ftz* stripe boundary points sampled on a cylindrical grid at each of the 14 stripe boundaries and 40 points uniformly spread in angle around the D-V axis. We extracted edges of each reference gene pattern in cylindrical coordinates by finding local maxima in the response of an anisotropic Gaussian derivative filter, which was elongated by a factor of three along the D-V direction. At a fixed threshold, this filter typically detected all the stripe boundaries but also yielded some outliers and an occasional missed detection due to variability in the staining.

To deal robustly with these errors, we performed an optimization along each of 40 A-P strips to match the 14 stripe boundaries in our template with the edges in the PointCloud. This 1D alignment between the template coordinates and the detected edges was carried out using dynamic programming on a cost function that depended on the polarity of the edge being matched (whether it is the anterior or posterior edge of a stripe) and the total displacement necessary to align the model along the strip. While this enforced consistency of matches along the A-P axis (e.g., two stripes in a template cannot be matched to the same stripe in the embryo), neighboring A-P strips could still be inconsistent. Before estimating a warping, we performed a postprocessing step using a global quadratic cost to prune matches that were inconsistent with their neighbors in either the A-P or D-V directions (see Supplemental Data).

Modeling Deformations

We modeled deformations using the regularized thin-plate spline (TPS) (Duchon, 1977; Wahba, 1990). The TPS describes a smooth warping $u : \Re^3 \rightarrow \Re^3$ that maps detected boundary points $\{s^{m(1)}, s^{m(2)}, s^{m(3)} \ldots\}$ to their respective targets in the template $\{t^1, t^2, t^3 \ldots\}$. We treat each coordinate of the function $u = (u_1, u_2, u_3)$ separately, and solve for the regularized multivariate spline that minimizes the functional:

$$J(u_i) = \sum_j \left\| u_i(s^{m(j)}) - t_i^j \right\|^2 + \lambda \sum_{j,k,l=1}^{3} \int \left(\frac{\partial^3 u_i(x)}{\partial x_j \partial x_k \partial x_l} \right)^2 dx$$

Although u_i is infinite-dimensional, the optimal solution can be specified in closed form with coefficients given by the solution of a compact system of linear equations (Wahba, 1990).

The regularized TPS provides a free parameter λ that trades off the fidelity of the warping u at the marker points with the smoothness of the interpolation throughout the remainder of the embryo. We set this parameter by crossvalidation, choosing the value that minimized the apparent interembryo variability on nonmarker genes. We also used this same validation technique to compare TPS to other deformation models. For example, we found that TPS removed 10%–20% more variability than Gaussian radial basis function splines at the optimal parameter settings.

Normalizing Expression Levels

Our analyses assumed that the total expression level of a gene was the same between embryos in the same cohort, and that the fluorescence levels measured in different batches were related by a single multiplicative factor. We used embryos from different developmental time points that were fixed and hybridized in a single batch in order to estimate the temporal progression of the 99th percentile expression level. When more than one hybridization was available for a given gene, we estimated a scale parameter for each batch in order to minimize the squared error relative to the mean. Since the absolute expression level between different genes is not calibrated in a meaningful way, we scaled expression so that the maximum average expression recorded for each gene over the entire time interval was 1.0. These scaled measurements were smoothed using Gaussian process regression (Rasmussen and Williams, 2006) to yield the expression time courses plotted as dotted lines in Figure S3. We used a squared exponential covariance function with characteristic length scale of 3 cohorts (roughly 30 min) and independent noise model with standard deviation of 0.3. Once the max expression level for each gene and cohort was estimated, a gain and offset was chosen for each embryo that minimized the variability within the cohort while matching the time course max.

Fitting Regulatory Functions

In our regression experiments, we used a generic form for the regulatory function F consisting of a sigmoid applied to a linear combination of transcription factor concentrations

$$F(P \mid a, b) = \frac{1}{1 + e^{a^T P + b}},$$

where P is the vector of protein concentrations and a,b are model parameters. The sigmoid provides a saturating, nonlinear response that constrains the transcription rate to lie between 0 and a maximum (scaled to 1) and can be motivated in part from thermodynamic considerations (Mjolsness, 2007; Bintu et al., 2004). The parameter vector a determines the steepness of the response to each factor, while b sets the offset at which transcription reaches half of the maximum value. We also considered a similar model for F, which included quadratic terms (products of all pairs of protein concentrations). While providing higher-quality fits (not shown), such a model results in a far greater number of parameters that are difficult to interpret, so we preferred the more parsimonious linear model used in the experiments described here.

To fit the parameters a and b to our observed data, we perform least-squares minimization over all nuclei at all time points for which we have data, as given by

$$C = \min_{a,b} \sum_{x,t} \left\| M(x,t) - F(P(x,t) \mid (a,b) \right\|^2,$$

where M(x,t) is the measured mRNA transcription of a given target gene in blastoderm nucleus x at time t and P(x,t) is the corresponding vector of protein concentrations. This optimization was subject to the constraint that only six entries in a could be nonzero. We characterized the goodness of fit for each target using $R^2 = 1 - \frac{C}{Var(M)}$, which measures the extent to which the model explains the variance in expression across measured nuclei and time points.

SUPPLEMENTAL DATA

Supplemental Data include eight figures, one table, and Supplemental References and can be found with this article online at http://www.cell.com/cgi/content/full/133/2/364/DC1/.

ACKNOWLEDGMENTS

This work is part of a broader collaboration by the BDTNP. We are grateful for the frequent advice, support, criticisms, and enthusiasm of its members. We thank Thomas Gregor and William Bialek for insightful discussions on variability. Work conducted by the BDTNP is funded by a grant from NIGMS and NHGRI, GM704403, at Lawrence Berkeley National Laboratory under Department of Energy contract DE-AC02-05CH11231.

Received: May 25, 2007
Revised: November 27, 2007
Accepted: January 31, 2008
Published: April 17, 2008

REFERENCES

Arnosti, D.N., Barolo, S., Levine, M., and Small, S. (1996). The eve stripe 2 enhancer employs multiple modes of transcriptional synergy. Development *122*, 205–214.

Azevedo, R., French, V., and Partridge, L. (1996). Thermal evolution of egg size in *Drosophila Melanogaster*. Evolution Int. J. Org. Evolution *50*, 2338–2345.

Bintu, L., Buchler, N.E., Garcia, H.G., Gerland, U., Hwa, T., Kondev, J., and Phillips, R. (2004). Transcriptional regulation by the numbers: models. Curr. Opin. Genet. Dev. *15*, 116–124.

Clyde, D.E., Corado, M.S., Wu, X., Pare, A., Papatsenko, D., and Small, S. (2003). A self-organizing system of repressor gradients establishes segmental complexity in Drosophila. Nature *426*, 849–853.

Duchon, J. (1977). Splines Minimizing Rotation-Invariant Semi-Norms in Sobolev Spaces. In Constructive Theory of Functions of Several Variables, W. Schempp and K. Zeller, eds. (Berlin: Springer-Verlag), pp. 85–100.

Edgar, B.A., Kiehle, C.P., and Schubiger, G. (1986). Cell cycle control by the nucleo-cytoplasmic ratio in early *Drosophila* development. Cell *44*, 365–372.

Eldon, E.D., and Pirrotta, V. (1991). Interaction of the Drosophila gap gene giant with maternal and zygotic pattern-forming genes. Development *111*, 367–378.

Fowlkes, C.C., and Malik, J. (2006). Inferring nuclear movements from fixed material. Report no. UCB/EECS-2006–142. http://www.eecs.berkeley.edu/Pubs/TechRpts/2006/EECS-2006-142.pdf.

Gregor, T., Tank, D.W., Wieschaus, E.F., and Bialek, W. (2007). Probing the limits to positional information. Cell *130*, 153–164.

Janssens, H., Hou, S., Jaeger, J., Kim, A., Myasnikova, E., Sharp, D., and Reinitz, J. (2006). Quantitative and predictive modeling of transcriptional control of the Drosophila melanogaster even skipped gene. Nat. Genet. *38*, 1159–1165.

Jaeger, J., Surkova, S., Blagov, M., Janssens, H., Kosman, D., Kozlov, K.N., Manu, Myasnikova E, Vanario-Alonso, C.E., Samsonova, M., Sharp, D.H., et al. (2004). Dynamic control of positional information in the early Drosophila embryo. Nature *430*, 368–371.

Keränen, S.V.E., Fowlkes, C.C., Luengo Hendriks, C.L., Sudar, D., Knowles, D.W., Malik, J., and Biggin, M.D. (2006). 3D morphology and gene expression in the Drosophila blastoderm at cellular resolution II: dynamics. Genome Biol. *7*, R124.

Kudoh, T., Tsang, M., Hukriede, N.A., Chen, X., Dedekian, M., Clarke, C.J., Kiang, A., Schultz, S., Epstein, J., Toyama, R., and Dawid, I. (2001). A gene expression screen in zebrafish embryogenesis. Genome Res. *11*, 1979–1987.

Kosman, D., Mizutani, C.M., Lemons, D., Cox, W.G., McGinnis, W., and Bier, E. (2004). Multiplex detection of RNA expression in Drosophila embryos. Science *305*, 846.

Laney, J.D., and Biggin, M.D. (1996). Redundant control of *Ultrabithorax* by *zeste* involves functional levels of zeste binding at the *Ultrabithorax* promoter. Development *122*, 2303–2311.

Lein, E.S., Hawrylycz, M.J., Ao, N., Ayres, M., Bensinger, A., Bernard, A., Boe, A.F., Boguski, M.S., Brockway, K.S., Byrnes, E.J., et al. (2007). Genome-wide atlas of gene expression in the adult mouse brain. Nature *445*, 168–176.

Ludwig, M., Palsson, A., Alekseeva, E., Bergman, C., Nathan, J., and Kreitman, M. (2005). Functional evolution of a cis-regulatory module. PLoS Biol. *3*, 588–598.

Luengo Hendriks, C.L., Keränen, S.V.E., Fowlkes, C.C., Simirenko, L., Weber, G.H., Henriquez, C., Kaszuba, D.W., Hamann, B., Eisen, M.B., Malik, J., et al. (2006). 3D morphology and gene expression in the Drosophila blastoderm at cellular resolution I: data acquisition pipeline. Genome Biol. *7*, R123.

Mjolsness, E. (2007). On cooperative quasi-equilibrium models of transcriptional regulation. J. Bioinform. Comput. Biol. *5*(2B), 467–490.

Myasnikova, E., Samsanova, A., Kozlov, K., Samsonova, M., and Reinitz, J. (2001). Registration of the expression patterns of *Drosophila* segmentation genes by two independent methods. Bioinformatics *17*, 3–12.

Oliveri, P., and Davidson, E.H. (2004). Gene regulatory network controlling embryonic specification in the sea urchin. Curr. Opin. Genet. Dev. *14*, 351–360.

Rasmussen, C., and Williams, C. (2006). Gaussian Processes for Machine Learning (Boston: MIT Press).

Rübel, O., Weber, G.H., Keränen, S.V.E., Fowlkes, C.C., Luengo Hendriks, C.L., Shah, N.Y., Biggin, M.D., Hagen, H., Knowles, D.W., Malik, J., et al. (2006). PointCloudXplore: Visual analysis of 3D gene expression data using physical views and parallel coordinates. In Data Visualization 2006: Proceedings of the Eurographics/IEEE-VGTC Symposium on Visualization, B.C. Santos, T. Ertl, and K. Joy, eds. (Lisbon, Portugal: EuroVis 2006).

Small, S., Blair, A., and Levine, M. (1992). Regulation of even-skipped stripe 2 in the Drosophila embryo. EMBO J. *11*, 4047–4057.

Spirov, A., Kazansky, A., Timakin, D., and Reinitz, J. (2002). Reconstruction of the dynamics of *Drosophila* genes expression from sets of images sharing a common pattern. Real-Time Imaging *8*, 507–518.

Struffi, P., Corado, M., Kulkarni, M., and Arnosti, D.N. (2004). Quantitative contributions of CtBP-dependent and -independent repression activities of Knirps. Development *131*, 2419–2429.

Tassy, O., Daian, F., Hudson, C., Bertrand, V., and Lemaire, P. (2006). A quantitative approach to the study of cell shapes and interactions during early chordate embryogenesis. Curr. Biol. *16*, 345–358.

Tomancak, P., Berman, B.P., Beaton, A., Weiszmann, R., Kwan, E., Hartenstein, V., Celniker, S.E., and Rubin, G.M. (2007). Global analysis of patterns of gene expression during Drosophila embryogenesis. Genome Biol. *8*, R145.

Turner, F.R., and Mahowald, A.P. (1976). Scanning electron microscopy of Drosophila embryogenesis. Dev. Biol. *50*, 95–108.

Visel, A., Thaller, C., and Eichele, G. (2004). GenePaint.org: An atlas of gene expression patterns in the mouse embryo. Nucleic Acids Res. *32*, D552–D556.

Wahba, G. (1990). Spline Models for Observational Data (Montpelier, VT: SIAM).

Warren, D.C. (1924). Inheritance of egg size in *Drosophila melanogaster*. Genetics *9*, 41–69.

Weber, G.H., Rübel, O., Huang, M.-Y., DePace, A.H., Fowlkes, C.C., Keränen, S.V.E., Luengo Hendriks, C.L., Hagen, H., Knowles, D.W., Malik, J., et al. (2008). Visual exploration of three-dimensional gene expression using physical views and linked abstract views. IEEE/ACM Trans. Comput. Biol. Bioinform. Published online March 31, 2008. 10.1109/TCBB.2007.70249.

Yuh, C.H., Bolouri, H., and Davidson, E.H. (2001). Cis-regulatory logic in the endo16 gene: switching from a specification to a differentiation mode of control. Development *128*, 617–629.

Zalokar, M., and Erk, I. (1976). Division and migration of nuclei during early embryogenesis of Drosophila melanogaster. J. Micro. Cell. *25*, 97–106.